JOURNAL OF AIRCRAFT
Vol. 42, No. 3, May–June 2005

Recommendations for Computational-Fluid-Dynamics Procedures for Predicting Abrupt Wing Stall

S. H. Woodson,* B. E. Green,† J. J. Chung,† and D. V. Grove†
U.S. Naval Air Systems Command, Patuxent River, Maryland 20670
P. C. Parikh*
NASA Langley Research Center, Hampton, Virginia 23681
and
J. R. Forsythe‡
U.S. Air Force Academy, Colorado Springs, Colorado 80840

This paper summarizes the lessons learned from the computational-fluid-dynamics effort of the joint NASA/Navy/Air Force Abrupt Wing Stall Program, discusses the results, and makes recommendations for approaches to be used in future aircraft programs to identify uncommanded lateral characteristics early in the design phase of an aircraft development program. The discussion also suggests procedures and figures of merit for use in predicting and quantifying rapid and severe wing-stall tendencies and vulnerabilities of the proposed designs. Topics addressed include critical parameters that can be used to identify uncommanded lateral activity in the transonic flow regime and the geometric parameters that were the primary contributors to the adverse lateral activity observed on preproduction F/A-18E/F aircraft. In addition, differences in steady-state and averaged time-accurate computational solutions for the F/A-18E in the abrupt-wing-stall region of interest are analyzed and compared with existing unsteady experimental data to determine the utility and accuracy of the unsteady approach. Lastly, proposed computational figures of merit are critically evaluated as indicators of possible abrupt separation tendencies, and screening procedures for the identification of those tendencies are suggested.

Introduction

THE goal of the computational-fluid-dynamics (CFD) efforts for the Abrupt Wing Stall (AWS) Program was to provide insight into the physical flow mechanisms that cause a wing to experience a rapid and severe upper-surface flow separation in the region of maximum lift. In addition, an attempt was made to derive easily obtainable computational figures of merit (FOM), which could be utilized early in an aircraft development program to alert engineers that the design may be susceptible to an abrupt stall in the transonic regime. Various FOM have been developed for the identification of AWS, and the relative merits of each are evaluated herein. The CFD research was conducted in coordination, with and parallel to, an extensive and complimentary experimental program to determine the relevant aerodynamic characteristics of four modern fighter and attack aircraft that routinely operate near, at, and above wing stall in the transonic regime. Two of the aircraft configurations considered in the study are susceptible to AWS (preproduction F/A-18E, and the AV-8B at the limits of its operational envelope), and two are not (F/A-18C, F-16C). These four configurations were chosen to evaluate the general utility of the various computational (and experimental) FOM for predicting the onset and severity of an AWS event. It was hoped that reliable FOM could be developed which would indicate where in the angle-of-attack (AoA) range a given configuration would experience an AWS event for a specified Mach number.

To be of predictive value, the candidate FOM developed in this program must "flag" in regions of known AWS or wing drop/wing rock for the F/A-18E and the AV-8B, yet remain docile outside that region. Further, the FOM should not flag for the F/A-18C and F-16C throughout their transonic operating envelope when on flap schedules as used in normal operations. However, the results of the AWS studies indicate that both the F/A-18C and F-16C can be made to experience AWS for certain combinations of Mach and AoA off of flap schedule; so to be robust and reliable, the FOM should flag in those conditions also.

Numerous CFD codes have been employed during the four years of the AWS Program. This paper will address the results obtained from three of the most popular Navier–Stokes (N-S) codes in use today by the engineering community. One is the structured, chimera code WIND[1] and the other two are the unstructured codes Cobalt[2] [the commercial version originally developed under the aegis of the U.S. Department of Defense (DoD)-CHSSI[3] program] and the USM3D[4,5] code developed at the NASA Langley Research Center. The utility of each of these three codes to model accurately the complex flowfield in the transonic AWS region of interest for fighter and attack aircraft has been discussed previously.[6] Here, we critically examine the results obtained, propose and evaluate computational FOM, and suggest techniques and procedures that aircraft designers can employ to identify whether or not their aircraft design will be susceptible to AWS.

Complexity of AWS Prediction

In this paper, we are concerned with the complexities of simulating the aircraft geometries and the extremely complicated flow field, which is developed about the vehicle when it is operated during strenuous maneuvers in the transonic regime. As an example of the complex flowfields to be computed, Fig. 1 shows a typical Cobalt solution[6] for an F/A-18C operating at a Mach number of 0.9 and an AoA of 9 deg. Only one side of the aircraft was modeled, utilizing a plane-of-symmetry boundary condition along the aircraft centerline. The leading-edge (LE) flap is deflected 6 deg, the trailing-edge (TE) flap is deflected 8 deg, and the aileron is not deflected. This flap configuration is denoted as flaps 6/8/0. The

Presented as Paper 2003-0923 at the AIAA 41st Aerospace Sciences Meeting, Reno, NV, 6–9 January 2003; received 18 June 2003; revision received 8 September 2003; accepted for publication 9 September 2003.

*Aerospace Engineer. Associate Fellow AIAA.
†Aerospace Engineer. Senior Member AIAA.
‡Associate Professor. Senior Member AIAA.

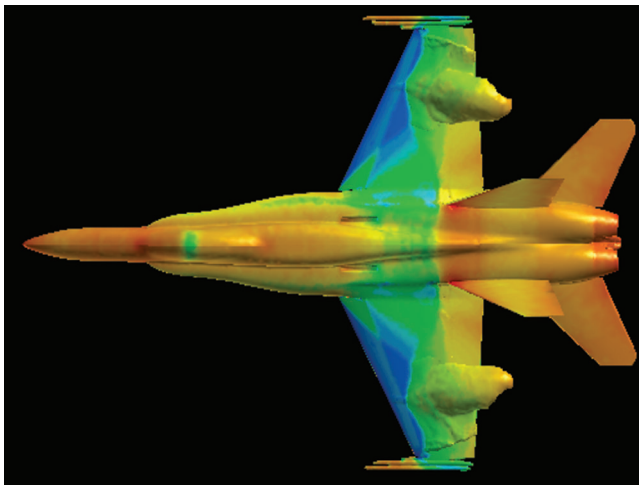

Fig. 1 Upper-surface flow over F/A-18C, flaps 6/8/0, at $M = 0.9$ and AoA = 9 deg.

aircraft surface pressures are color coded, where blue represents lower-pressure, higher-velocity airflow and green/yellow indicates higher-pressure, lower-speed flow.

Also shown in Fig. 1 are isosurfaces of zero chordwise velocity, which indicate regions of separated flow. The complexity of the flowfield is readily apparent from the merging oblique shock waves formed by the leading-edge extension (LEX)/ wing juncture, the deflected LE flap, and the juncture of the AIM-9 launch rail with the wing tip. These oblique shocks merge in the midspan region of the wing to form a normal shock wave of sufficient strength to cause a large flow separation on the upper surface forward of the aileron. Also apparent is the subsequent reacceleration of the flow and the nearly full-span normal shock wave formed just forward of the base of the vertical stabilizer. The imprint of the LEX vortex is clearly visible, as well as the shock formed on the crown of the canopy. In addition, regions of stagnant flow are visible at the nose of the aircraft, forward of the canopy, and at the root of the vertical tail.

Thus, for high-performance aircraft operating at near sonic speeds and close to maximum lift for the wing, the three-dimensional flow about the vehicle is characterized by merging oblique and normal shock waves, numerous vortices, and shock-induced, massively separated upper-surface flows. Successful prediction of this type of flowfield requires high-fidelity computational models with off-body grid spacing sufficient to resolve the various length scales in the boundary layer near the surface. The global situation is a compressible, viscously dominated, shock-induced, massively separated flow that cannot be accurately computed with anything less than a Reynolds-averaged Navier–Stokes (RANS) analysis.[6]

Sensitivity of AWS Flow Phenomena

The major difficultly for predicting AWS (either computationally or experimentally) is the rapidity with which it can occur and the large flow topology change that is manifested. Figure 2 illustrates the upper-surface flow on the wing of a preproduction F/A-18E computed using WIND for Mach 0.8 at AoA = 8 and 9 deg (Ref. 7). Once again, the higher velocity flow is shown in blue and the lower speed (mostly separated) flow is depicted in green/yellow. Also included are surface-restricted particle traces at a location just off the wing surface, which are analogous to experimental oil flow patterns.

For the condition of 8-deg AoA, there exists a large, nearly full-span flow separation just forward of the TE flap hinge line. For 9-deg AoA, the flow separation has jumped to the LE flap hinge line near the LE wing snag over just a 1-deg AoA increment. Note also the additional oblique shocks formed by the presence of the snag and the increased strength of the shocks and larger separation region compared with those computed for the F/A-18C.

Similar results were obtained for the AV-8B (Ref. 8), flaps 0/10/0 using the USM3D code for the conditions of Mach 0.75 and AoA = 6 and 7 deg, as shown in Fig. 3.

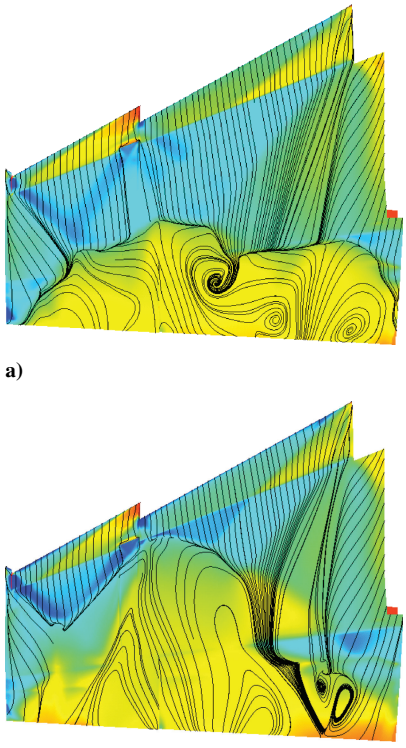

a)

b)

Fig. 2 Upper-surface flow over the F/A-18E, flaps 10/10/5 at $M = 0.8$ for a) 8-deg AoA and b) 9-deg AoA.

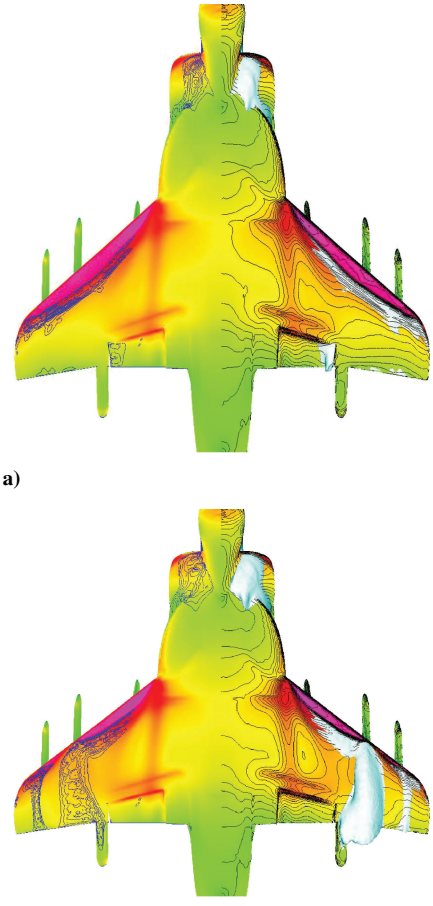

a)

b)

Fig. 3 Upper-surface flow over the AV-8B, flaps 0/10/0 at $M = 0.75$ for a) 6-deg AoA and b) 7-deg AoA.

In this figure, lower-pressure, higher-velocity flow is depicted in red, and the lower-speed, higher-pressure flow is shown as yellow/green. Also, now the isosurfaces of zero chordwise velocity are shown in white, but the characteristic is the same: there is a large difference in flow topology over only a 1-deg AoA change for a given configuration at a specific Mach number. At AoA = 6 deg, there is a small region of separation and reattachment along the span just aft of the shock along about 20% chord, whereas at 7-deg AoA there is suddenly a full-chord, large separated region in the vicinity of the midpylon and a secondary similar pattern behind the outboard pylon in front of the aileron.

CFD FOM

During the course of the AWS Program, several computational FOM were proposed and evaluated for their utility to either indicate a possible AWS event or predict at what conditions one might be anticipated. A secondary goal of the CFD FOM development was to provide the aircraft designer with a reliable indicator of potential uncommanded lateral problems for the proposed design, and perhaps, a means to identify the spanwise location where the event occurs and a quantitative measure of the severity of the phenomenon. This section describes some of the more promising FOM, which were derived in an attempt to meet those goals.

The first candidate FOM consisted of the character of the lift coefficient vs AoA curve, where a change in sign of the slope of the curve was apparent in the region where AWS was encountered in both wind-tunnel experiments[9] and flight tests for the F/A-18E. However, the change in sign of the lift-curve slope was found to be less of a reliable indictor of the onset of AWS when compared to the change in sign of the wing-root bending-moment coefficient[10]as illustrated in Fig. 4 for the F/A-18C at 0.8 and 0.9 Mach.

At 0.9 Mach the lift coefficient does not indicate a change in slope, whereas the C_{WB} curve shows a zero slope at 11-deg AoA. For 0.8 Mach, both curves show a slope change at 10-deg AoA, with a more pronounced break in the C_{WB} curve. The change in sign of the slope of the C_{WB} curve provides the added benefit in that it indicates a loss of roll damping[9] and therefore a possible propelling aerodynamic moment if rolling motions are initiated by asymmetries existing for that Mach/AoA region. Thus, the slope of the C_{WB} curve is a useful flag that can be utilized by an aircraft designer to look more carefully at the proposed design in the AWS region of interest to investigate adverse lateral motions.

Another obvious potential FOM is the variation of spanwise sectional lift coefficient with angle of attack. Historically, it is well known that in order to avoid unwanted lateral rolloffs near maximum lift the wing should be designed such that the inboard section stalls before the outer section. This goal is usually accomplished by differences between inboard and outboard incidence angles from the wing root to the tip (geometric twist) and the incorporation of changes in airfoil sections (aerodynamic twist). However, even for high-aspect-ratio, single-point design transport aircraft, this is not easily accomplished because of other structural, manufacturing, operational, and maintainable design considerations. As a result, designers have had to use aerodynamic "fixes" such as fences, vortex generators, stall strips, and other devices to ensure satisfactory handling characteristics near stall.

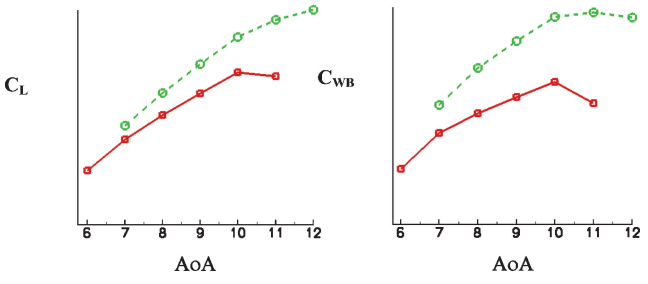

Fig. 4 Lift and wing-root-bending coefficient for the F/A-18C, flaps 6/8/0: —□—, Mach 0.8; and - -⊙- -, Mach 0.9.

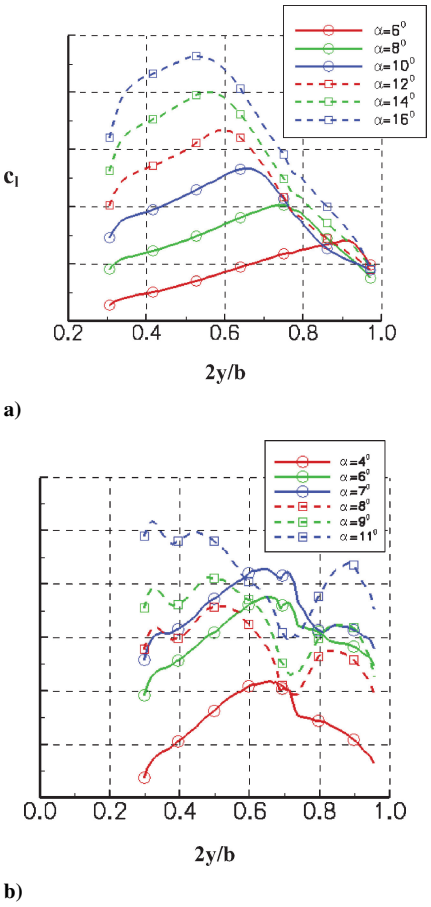

Fig. 5 Sectional lift coefficient vs span at $M = 0.9$ for a) the F-16C and b) the F/A-18E.

The design considerations for low-aspect-ratio, multipoint design fighter and attack aircraft are further constrained by the additional considerations imposed by low-observable and survivability requirements. Nonetheless, to ensure lateral control near wing stall (in whatever fashion) it is desirable to have the airflow attached in front of the ailerons throughout the operating envelope of the aircraft.

Contrast the sectional lift characteristics[11] between the F-16C and the F/A-18E presented in Fig. 5 for several AoA at Mach 0.9. As the AoA increases for the F-16C, the maximum wing loading moves inboard in a continuous, smooth manner, and the maximum sectional lift is achieved about midspan at the highest AoA.

The sectional lift curves for the F/A-18E, on the other hand, are nearly constant along the wing span for a given AoA and increase with increasing AoA until between 7 and 8 deg, where an abrupt, large loss of overall lift is observed in the vicinity of the LE snag. The LE snag on the F/A-18E is located at 72.5% of the span, and the increase of sectional lift caused by the increased chord outboard of the snag can clearly be seen in Fig. 5. For this combination of Mach and AoA (between 7 and 8 deg), the F/A-18E with flaps 10/10/5 was observed to experience an AWS event in the NASA Langley Research Center's 16-Foot Transonic Tunnel utilizing the newly developed free-to-roll rig.[12] This uncommanded motion correlates very well to a wing-drop event experienced by the preproduction F/A-18E aircraft during engineering and manufacturing development flight tests.

A composite FOM for indicating the onset of AWS has been developed,[10] which consists of the sectional lift coefficient and its derivative with respect to AoA plotted along the wing span. The quantification of the abruptness of lift loss is thought to be a measure of the sensitivity of the wing configuration to uncommanded roll. This parameter has proven to be a reliable indicator of the onset of AWS for each of the aircraft configurations considered in this study

and provides numerous insights into where the problem occurs, both in terms of AoA and location along the wingspan.[8,10,11] Figures 6 and 7, taken from Ref. 10, show plots of the sectional lift coefficient and its derivative with respect to AoA for two different aircraft configurations.

Figure 6 gives the results for the baseline F/A-18C, and Fig. 7 presents the results for the baseline F/A-18C with the addition of a LE snag of the same normalized dimensions and location as that used on the F/A-18E. The dip in the sectional lift curves for the F/A-18C occurring around 70% span are caused by the difference between the deflected TE flap and the undeflected aileron.

As was the case for the F-16C, as AoA is increased, overall lift is increased, and the center of lift along the span moves inboard. The addition of a LE snag to the baseline F/A-18C produces a localized increase in lift and moves the center of lift slightly outboard, which promotes flow separation in that area because of the increased local lift. Careful examination of the sectional lift curves between 9- and 9.5-deg AoA for the F/A-18C with a LE snag reveals a loss of lift in the region of the LE snag (72.5% span). As a predictive FOM of AWS, this characteristic is not a very good indicator. However, consider in addition the derivative of the sectional lift coefficient with respect to AoA. There is a significant loss of lift between 9 and 9.5 deg as indicated in Fig. 7b.

Although the change in slope of the C_{WB} curve has been shown previously to be a more reliable indicator of AWS than the slope of the lift curve, Parikh and Chung[11] have shown that the half-plane rolling-moment coefficient C_l provides identical information, as illustrated in Fig. 8. Thus, the same indication of potential adverse activity can be obtained prior to performing a spanwise integration of the sectional lift. This could serve as an early flag for AWS in that the rolling moment is one of the basic outputs of any CFD code.

However, as we have seen, numerous insights can be gained by calculating the wing-root bending-moment coefficient. Green and Ott[10] provide an excellent example of the utility of C_{WB} for quantifying the effect of various geometric parameters contributing to AWS. During their study, they systematically varied each of the wing design parameters that were incorporated into the design of the F/A-18E, which differed from the F/A-18C (e.g., removal

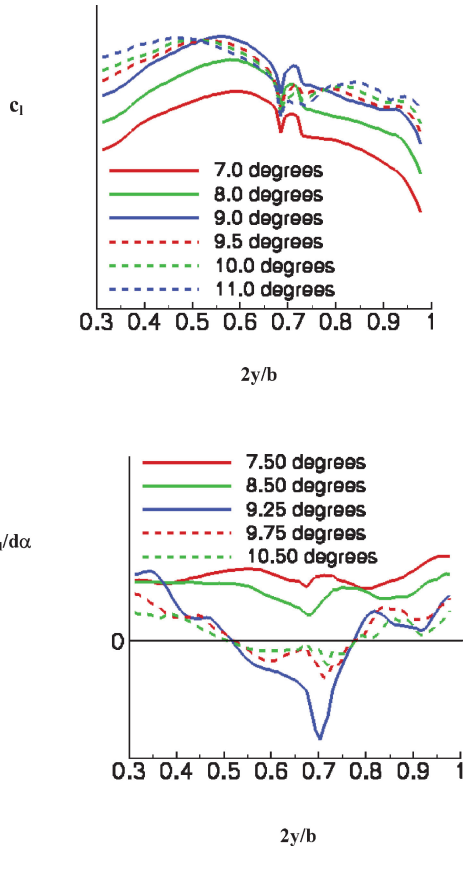

Fig. 7 Sectional lift coefficient and its derivative with respect to AoA for the baseline F/A-18C with a LE snag, flaps 6/8/0 at $M = 0.9$.

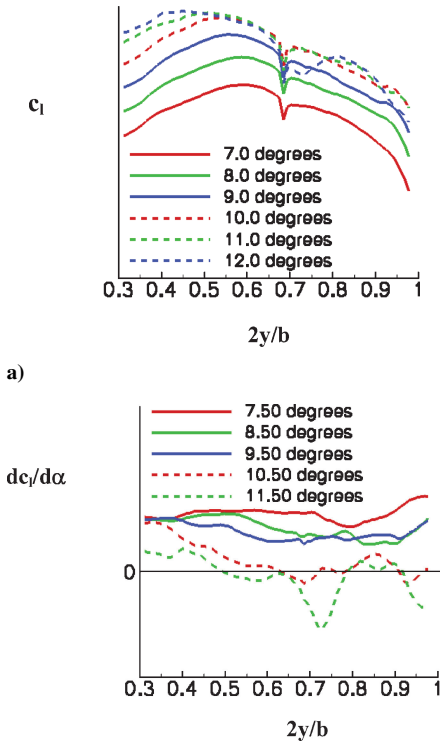

Fig. 6 Sectional lift coefficient and its derivative with respect to AoA for the baseline F/A-18C, flaps 6/8/0 at $M = 0.9$.

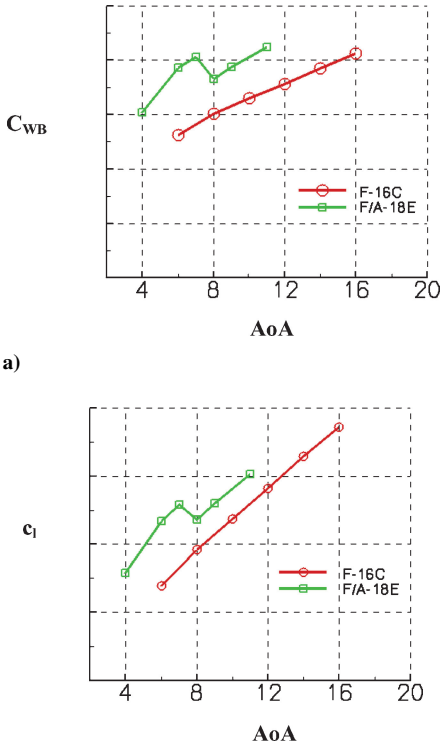

Fig. 8 Equivalency of the wing-root bending-moment and half-plane rolling-moment coefficients at $M = 0.8$.

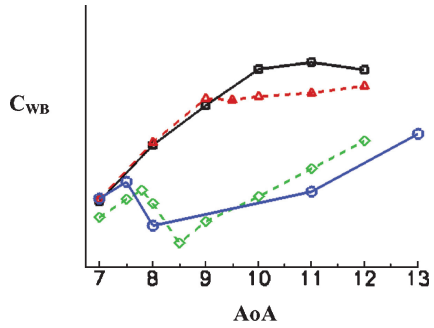

Fig. 9 Wing-root-bending coefficient vs AoA for baseline F/A-18C, preproduction F/A-18E, and two morphed configurations: —□—, F/A-18C[1]; - -□- -, F/A-18C with snag and tapered LE flap[1]; and - -△- -, F/A-18C with snag[1]; —○—, F/A-18E,[2] with [1]Mach 0.9, $Re = 2.07 \times 10^6$, 6-deg/8-deg/0-deg flaps and [2]Mach 0.9, $Re = 3.14 \times 10^6$, 6-deg/8-deg/4-deg flaps.

of outboard twist). They determined that the two most significant contributors were the addition of a wing leading-edge snag and the reduction in the leading-edge flap-chord ratio as shown in Fig. 9. The addition of a LE snag to the baseline F/A-18C reduces the overall lift and moves the local maximum to a lower AoA. Reducing the leading-edge flap chord in addition to the inclusion of the snag produces more dramatic results, and that morphed configuration has very similar characteristics to the preproduction F/A-18E.

Steady Versus Time-Averaged Unsteady CFD

During wind-tunnel testing of a highly instrumented preproduction F/A-18E model in the NASA Langley 16-Foot Transonic Tunnel, very severe model dynamics were observed for certain combinations of Mach number and AoA as reported by Schuster and Byrd.[12] The unsteadiness was of such an extent that data could not be recorded, and operational test safety became a concern. At slightly lower angles of attack, unsteady shock fluctuations were experienced, as has been noted for other studies of wings at transonic, separated flow conditions. The left wing panel of the F/A-18E model was instrumented with a total of 23 unsteady pressure transducers. A typical example of the upper-surface-pressure distribution in an area near the snag is shown in Fig. 10. The blue line represents the time average of the instantaneous pressures (1000 samples/s for 10 s). The green symbols are the minimum value of the pressure coefficient, and the red symbols represent the maximum. As can be seen in the figure, significant chordwise shock motion is apparent (20–40% chord). The mean pressure distribution is smeared as a result of averaging of a sharp oscillating shock wave (seen by observing the instantaneous pressure distributions). This is a difficult effect for RANS models to capture because they are designed to predict the mean flow and are calibrated on simple building-block flows such as boundary and shear layers. Sometimes they can predict unsteady effects caused by separations, but this is far from their calibration range. Unsteady RANS calculations sometimes pick up unsteadiness caused by separation and can provide better agreement.

One of the shortcomings of applying steady-state CFD (RANS) to this problem was that the models tended to overpredict the lift and miss the shock location.[6] It was therefore decided to attempt an unsteady calculation in order to determine if the unsteady shock motion could be captured by CFD. RANS models were run as time accurate, but failed to give any significant shock motion. This failure motivated Forsythe and Woodson[13] to apply the detached-eddy simulation (DES) turbulence model developed by Spalart et al.[14] using the Cobalt N-S code. DES is a hybrid Reynolds-averaged Navier–Stokes and large-eddy simulation (LES) model. The model is design for accurate prediction of massively separated flows at flight Reynolds numbers by applying RANS in the boundary layer where it is economically feasible and LES in the separated regions. Some results of the DES calculations are provided Figs. 10–12 taken from Ref. 13. Simulations were performed on a baseline grid and a

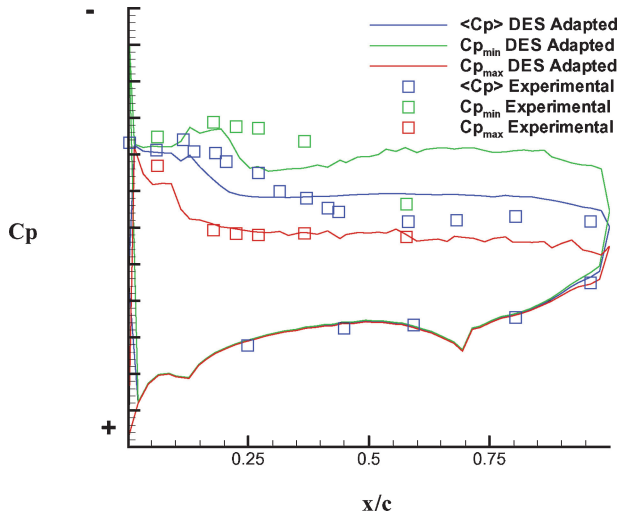

Fig. 10 Upper-surface-pressure coefficient distribution near midspan for the F/A-18E, flaps 10/10/5 at $M = 0.9$ and AoA = 8.5 deg.

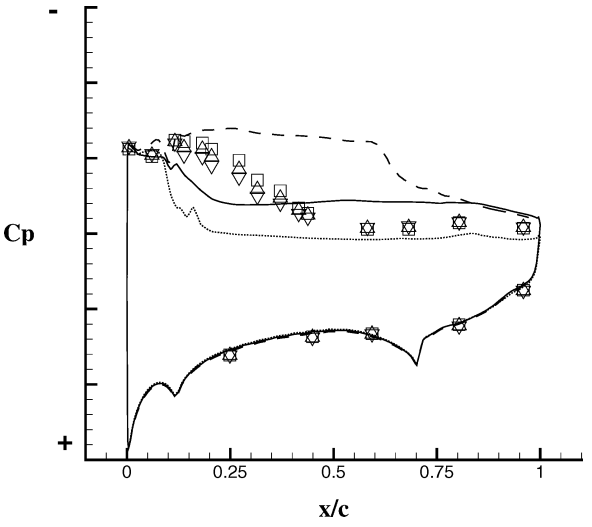

Fig. 11 Steady-state vs time-averaged pressure coefficient distribution near midspan for the F/A-18E, flaps 10/10/5 at $M = 0.9$ and AoA = 9 deg: ——, DES, 9 deg, adapted; – – –, SA, 9 deg, baseline; . . . ., SST, 9 deg, baseline; ∇, run 20, $\alpha = 8.92$ deg; △, run 19, $\alpha = 8.91$ deg; and □, run 18, $\alpha = 8.91$ deg.

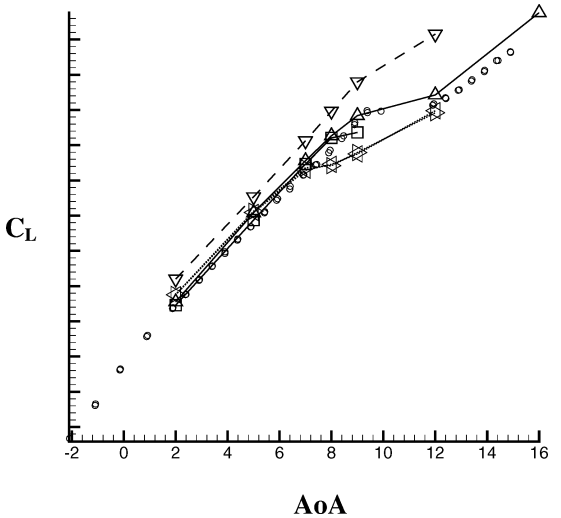

Fig. 12 Steady-state vs time-averaged lift coefficient for the F/A-18E, flaps 10/10/5 at $M = 0.9$: —□—, DES baseline; —△—, DES adapted; -∇- -, SA baseline; ··▷··, SST baseline; ··◁··, SST adapted; and ○, experimental.

solution adapted grid. Figure 10 compares the min, max, and average pressure coefficients for the DES calculations on the adapted grid to the experiments already described. The range of shock motion is underpredicted in the DES, but shock motion is clearly present and in close to the right position.

Figure 11 presents the time-averaged DES result for the upper-surface-pressure distribution near midspan compared with the experimental data as well as the steady-state results obtained from both a one-equation and two-equation turbulence model. A distinct feature of both of the RANS solutions is the sharpness of the shocks, with SA predicting a shock location about 70% chord, while the SST result is at about 12% chord. The advantage of the DES calculation is that it is an average of a moving shock, and thus the shock location is smeared, and much better agreement with the experimental data is obtained. Although none of the models are in perfect agreement with the experiments, it should be kept in mind that in the experiments the shock traveled from the trailing edge to the leading edge with only a few degrees change in AoA. Therefore the shock location is very sensitive to small disturbances, which is a likely contribution to its unsteadiness and the difficulty in predicting the mean shock location with CFD.

A comparison of the lift coefficient between the RANS results with the DES solution for the F/A-18E is shown in Fig. 12. If one compares Fig. 11 with Fig. 12, it is readily apparent why the SA solution overpredicts the lift in the AWS region, and why the SST results underpredict the lift. The DES results are in much closer agreement with the experimental data, and grid adaptation improves the result by providing more resolution in the LES region, which reduces modeling errors. The DES result is about 5–10 times more expensive than the steady-state RANS solutions.

Screening Procedures for AWS Using CFD

In the preliminary design of a new air vehicle, it is impractical employ full Navier–Stokes analysis (at present) while performing trade studies. However, after an initial design has been frozen and wind-tunnel models of the proposed design are being fabricated, it is eminently possible with today's parallel codes and multiprocessor computers to perform a N-S analysis for a few Mach numbers and to have the results prior to the tunnel entry. A recommended AWS screening approach would consist of four steps:

1) Construct a CFD grid of the half-plane aircraft of sufficient density to adequately resolve the boundary layer for full-scale Reynolds numbers in the transonic regime. The same grid model can then be used to compare results with the wind-tunnel data and to determine Reynolds-number effects.

2) Utilize the computational FOM to identify potential AWS indicators. The FOM can be thought of as "red flags," which require more careful or detailed attention.

3) Modify the geometry to minimize or eliminate the red flags and rerun selected cases in the AWS region of interest.

4) When candidate modifications have been identified and analyzed, verify the CFD predictions by wind-tunnel testing a prudently instrumented model of the redesign. Beneficial instrumentation would include wing-root-bending gauges on both wing panels and as many static and unsteady pressure taps as the model size will allow.

Recommendations

Based on the results of the CFD efforts from the AWS Program, specific recommendations for identifying and mitigating AWS are as follows:

1) As soon as practical, create a viscous semispan grid with a $y^+ = 1$ and generate a RANS transonic polar. This approach is not only a good idea for identifying potential adverse activity, but it can also provide $C_{L\max}$, spillage, jet effects, cruise drag, inlet pressure recovery, hinge moments, etc.

2) Look for slope changes in the lift and half-plane rolling moment vs AoA curves. Changes in slope or local maximums (especially large or abrupt changes) are initial red flags of possible problems.

3) Compute wing-root bending-moment coefficients and look for slope changes. A large, abrupt negative slope in the C_{WB} curve indicates an abrupt stall that could result in a large static rolling-moment asymmetry, and the negative slope also implies a loss of aerodynamic roll damping.

4) In regions of local $C_{L\max}$, compute solutions in smaller AoA increments to identify the severity of the break. Too large an AoA increment (greater than about 0.5 deg) can completely miss the AWS region of interest for high transonic Mach numbers.

5) Compute sectional C_l across the semispan and its derivative with respect to AoA. Higher loading mid- to outboard, rather than inboard, could cause AWS. The sectional lift derivative with AoA also quantifies the severity of the problem and indicates regions along the wing where the abrupt stall is occurring and modifications might be required.

6) Examine sectional pressure coefficient vs x/c at various locations along the wing span to look for where strong shock-induced separated regions are present. Large chordwise shock-induced separation can lead to unsteady flow and abrupt fore and aft shock movement.

7) If large regions of flow separation are present, time-accurate CFD calculations might be required to describe the flow accurately. Averaged time-accurate solutions provide improved mean-flow predictions and can be used to compute shock motion and the magnitude and frequency of the unsteady rolling moment. Low-frequency, large-magnitude oscillations could be a contributor to AWS.[13]

Summary

Several CFD flow solvers were successfully applied to the problem of transonic abrupt wing stall. The flowfield is characterized by massively separated shock-induced flow and requires at least a RANS analysis to compute accurately. In addition, computational figures of merit for identifying and quantifying the severity of the event were developed and the relative merits of each were evaluated. Finally, a screening method and specific recommendations of what to look for to identify the potential existence of uncommanded lateral activity were provided, which can be utilized by future aircraft development programs to evaluate if their design is susceptible to abrupt wing stall.

Acknowledgments

The authors wish to express their gratitude to Lawrence Ash of the Office of Naval Research for sponsoring this research. We would also like to thank the other members of the AWS Program team, particularly Joe Chambers, Joe Laiosa, and Bob Hall for many fruitful discussions. Of course, none of the results obtained would have been possible without the support and CPU hours provided by the Department of Defense High-Performance Computing Modernization Office.

References

[1]Bush, R. H., Power, G. D., and Towne, C. E., "WIND: The Production Flow Solver of the NPARC Alliance," AIAA Paper 98-0935, Jan. 1998.

[2]Strang, W. Z., Tomaro, R. F., and Grismer, M. J., "The Defining Methods of Cobalt$_{60}$: A Parallel, Implicit, Unstructured Euler/Navier–Stokes Flow Solver," AIAA Paper 99-0786, Jan. 1999.

[3]Common High-Performance Software Support Initiative, Dept. of Defense, Washington, DC.

[4]Frink, N. T., "Tetrahedral Unstructured Navier–Stokes Method for Turbulent Flows," *AIAA Journal*, Vol. 36, No. 11, 1998, pp. 1975–1982.

[5]Bhat, M. K., and Parikh, P. C., "Parallel Implementation of an Unstructured-Grid Based Navier–Stokes Solver," AIAA Paper 99-0663, Jan. 1999.

[6]Woodson, S. H., Green, B. E., Chung, J. J., Grove, D. V., Parikh, P. C., and Forsythe, J. R., "Understanding Abrupt Wing Stall with Computational Fluid Dynamics," *Journal of Aircraft*, Vol. 42, No. 3, 2005, pp. 578–585.

[7]Grove, D. V., Laiosa, J. P., Woodson, S. H., and Stookesberry, D. C., "Computational Fluid Dynamics Study of Abrupt Wing Stall Phenomena on the F/A-18E," AIAA Paper 02-1025, Jan. 2002.

[8]Chung, J. J., and Parikh, P. C., "A Computational Study of the Abrupt Wing Stall for Various Fighter Jets: Part II, AV-8B and F/A-18C," AIAA Paper 03-0747, Jan. 2003.

[9]Lamar, J., and Hall, R., "AWS Figure of Merit Developed Parameters from Static Transonic Model Tests," AIAA Paper 03-0745, Jan. 2003.

[10]Green, B. E., and Ott, J. D., "F/A-18C to E Wing Morphing Study for the Abrupt-Wing-Stall Program," *Journal of Aircraft*, Vol. 42, No. 3, 2005, pp. 617–626.

[11]Parikh, P. C., and Chung, J. J., "A Computational Study of the Abrupt Wing Stall for Various Fighter Jets: Part I, F/A-18E and F-16N," AIAA Paper 03-0746, Jan. 2003.

[12]Schuster, D., and Byrd, J., "Transonic Unsteady Aerodynamics of the F/A-18E Under Conditions Promoting Abrupt Wing Stall," *Journal of Aircraft*, Vol. 41, No. 3, 2004, pp. 485–492.

[13]Forsythe, J. R., and Woodson, S. H., "Unsteady Computations of Abrupt Wing Stall Using Detached-Eddy Simulation," *Journal of Aircraft*, Vol. 42, No. 3, 2005, pp. 606–616.

[14]Spalart, P. R., Jou, W. H., Strelets, M., and Allmaras, S. R., "Comments on the Feasibility of LES for Wings and on a Hybrid RANS/LES Approach," *Advances in DES/LES, 1st AFOSR International Conference on DES/LES*, Greyden Press, Columbus, OH, Aug. 1997.